Electronic Supplementary Information

DNA-inspired design of organic electrode materials for high-performance aqueous Zn-ion batteries

Liqiu Tang,[a,1] Mengpei Qi,[a,1] Chi-Pong Tsui,[c] Qing Zhang,[a] Chak-Yin Tang,[c] Yunhai Zhu,[*b] and Yingkui Yang[*a,b]

[a] Key Laboratory of Catalysis and Energy Materials Chemistry of Ministry of Education & Hubei Key Laboratory of Catalysis and Materials Science, South-Central Minzu University, Wuhan 430074, China

[b] State Key Laboratory of New Textile Materials and Advanced Processing, Wuhan Textile University, Wuhan 430200, China
Email: yhzhu@wtu.edu.cn (Y. Z.); ykyang@wtu.edu.cn (Y. Y.)

[c] Department of Industrial and Systems Engineering, The Hong Kong Polytechnic University, Hung Hom, Kowloon, Hong Kong, China

[1] These authors contributed equally to this work.

Correspondence and requests for materials should be addressed to Y. Z. and Y. Y. (yhzhu@wtu.edu.cn, ykyang@wtu.edu.cn).

1. Materials and Characterizations

***Materials*:** 2, 3-dichloro-1, 4-naphthoquinone (DCNQ) were procured from Energy Chemical. Potassium phthalimide were acquired from Shanghai Macklin Biochemical Co., Ltd. 1,4,5,8,9,11-Hexaazatriphenylenehexacarbonitrile (HAT-CN) were procured from Shanghai Rhawn Chemical Technology Co., Ltd. Phenazine (PNZ) were procured from Tianjin Heowns Biochemical Technology Co., Ltd. Anthraquinone (AQ) were procured from Shanghai Macklin Biochemical Co., Ltd. 5,10-Dihydrophenazine (DHPNZ) were acquired from Shanghai Macklin Biochemical Co., Ltd. Hydrazinium hydroxide solution (85%, AR) were acquired from Sinopharm Chemical Reagent Co., Ltd. N, N-Dimethylformamide (DMF) were acquired from Shanghai Aladdin Biochemical Technology Co. Ltd. Additionally, Polytetrafluoroethylene (PTFE, 60 wt%), Ketjin black (ECP-600JD) and zinc foil (99.99%) were obtained from Canrd Technology Co., Ltd. $ZnSO_4 \cdot 7H_2O$ (99%) was purchased from Sinopharm Chemical Reagent Co., Ltd. Glass fiber membrane (GF/D grade) was provided by Whatman company.

***Characterizations*:** FT-IR measurements were recorded on the Nicolet is50 spectrometer in the range of 600-3800 cm^{-1}. The structure was examined by solid-state ^{13}C NMR with Bruker Avance Neo 400WB. XPS measurements were performed on a Thermo Multi Lab 2000. The structure and phase composition were characterized by X-ray diffraction measurement (XRD, Rigaku D/Max 2400 using Cu/Kα radiation), and the diffraction data were collected at a step mode over the angular range of 5-50°. TGA was recorded on a NETZSCH (TG209F3) analyzer from 40-700 ℃ at a heating rate of 10 ℃ min^{-1} under nitrogen conditions. SEM images were taken on a Hitachi SU8010 microscope.TEM images and EDS mapping images were recorded on a Hitachi HT7700 electron microscope. The EPR spectrum was recorded on a Bruker EMXnano. Contact angle tests were recorded on DSA100 KRUSS Scientific. The liquid-state ^{1}H NMR and ^{13}C NMR were measured on 600 MHz Bruker Avance Neo. The Raman spectrum was recorded on a Thermo DXR. The mass spectra were measured on a UPLC-Q Exacitative MS.

Synthesis of DANQ. DANQ was synthesized with 2, 3-dichloro-1, 4-naphthoquinone and potassium phthalimide according to the previous report. Typically, 2, 3-dichloro-1, 4-naphthoquinone (7.5 g) was dissolved in acetonitrile (100 mL), and then potassium phthalimide (12.5 g) was added. The above solution was sonicated for 30 minutes to form a homogeneous solution. The mixture was stirred and

refluxed at 80 ℃ for 12 h under an Ar atmosphere. The yellow solids were collected via vacuum filtration accompanied by washing several times with hot DMF. The above powder was dried under a vacuum at 80 ℃ for 12 h and then transferred into a round-bottom flask. Subsequently, 50 mL of hydrazine hydrate was added. The above suspension was stirred at 60 ℃ for 6 h and collected by vacuum filtration via washing several times with water. Finally, the product was further purified by recrystallization from ethanol and then dried under a vacuum overnight.

Synthesis of HAT-NQ. A round bottom flask was charged with HAT-CN (61.6 mg,0.16 mmol), DANQ (90.2 mg,0.48 mmol), and Na_2CO_3 (100 mg), followed by 10 mL DMF. After stirring at room temperature for 1h, the mixture was refluxed and heated at 120 ℃ for 48 h under an N_2 atmosphere. After cooling to room temperature, the reaction solution was transferred to 300 mL of dilute hydrochloric acid solution and settled for 1 h. A black powder was achieved after washing by massive water, ethanol, DMF, and acetone, respectively. Finally, the resultant powder was further dried under a vacuum. The yield of HAT-NQ is 65.2%.

Electrochemical measurements. The electrodes were prepared by mixing active material, KB, and PTFE in a weight ratio of 6:3:1 by using ethanol absolute as solvent. The slurry was mixed homogeneously in solids under stirring for 20 min, and then the slurry was cast on stainless steel meshes. The electrodes were dried at 80 ℃ overnight under a vacuum. The electrode film is cut into round electrodes. Then, the active material mass of the pole pieces is calculated. The mass loading for the electrode is about 0.8-1.0 mg. The CR2032 coin cells were assembled in the air by using zinc foil and 2M aqueous $ZnSO_4$ as counter electrode and electrolyte, respectively. Glass fiber was used as a separator. For the pouch battery, the HAT-NQ membrane and Zn foil were cut to a size of 4 cm * 4 cm, respectively. Then, electrodes were prepared by connecting the HAT-NQ membrane pressed on soft stainless steel mesh and Zn foil with nickel lugs, respectively. The HAT-NQ electrode, glass fiber separator, and Zn foil electrode were stacked up to form a “sandwich” structure. The aqueous HAT-NQ//Zn pouch battery was obtained through a vacuum-sealed process after adding 2 M $ZnSO_4$ aqueous solution as an electrolyte. The electrochemical characteristics of the assembled cells underwent comprehensive evaluation employing diverse methodologies encompassing galvanostatic charge/discharge, electrochemical impedance spectroscopy (EIS), and cyclic voltammetry (CV).

Galvanostatic charge/discharge analyses encompassing various current densities were executed using a LAND-CT2001A battery testing instrument (LAND Electronic Co., Wuhan China) at a constant temperature of 25 ℃. CV measurements were conducted employing a CHI 660E (China) electrochemical workstation with a scan rate of 1 mV s^{-1}. EIS investigations were carried out within the frequency spectrum of 0.01-100,000 Hz, employing the same instrumentation and a voltage amplitude of 0.05 mV.

In situ attenuated total reflection infrared spectroscopy (ATR-IR) measurement. In-situ ATR-IR experiments were performed on an FT-IR spectrometer (INVENIO S, Bruker) equipped with an MCT-A detector. A slurry was prepared by mixing the active material, KB, and PTFE adhesive in a weight ratio of 6:3:1 in ethanol. A suitable amount of the slurry was then drop-coated onto a stainless steel mesh and dried to prepare a working electrode. The bottom of the in-situ cell was constructed using a ZnSe prism. The working electrode was placed on the back of the ZnSe prism, with Zn foil serving as the counter and reference electrodes. Glass fiber was used as the separator, and 2 M $ZnSO_4$ was used as the electrolyte. The ATR-IR spectra of the cathode were collected continuously every 2 minutes during discharge/charge processes in the potential range of 0.1-1.6 V (vs Zn^{2+}/Zn).

***Ex-situ measurement and sample preparation*:** During the *ex-situ* investigations of the electrode, coin cells underwent multiple charge and discharge cycles. Post-cycling, the coin cells were disassembled, and the electrodes obtained were cleansed using deionized water and subsequently dried under a vacuum before the ensuing testing procedures.

2. Computational details

DFT calculation: The HOMO, LUMO, and corresponding electrostatic potentials (ESP) of AQ, PNZ, DHPNZ, and HAT-NQ molecules were respectively calculated by the DMOL3 module in Materials Studio (MS) 2020. Firstly, the generalized gradient approximation (GGA) with Perdew–Burke–Ernzerhof (PBE) exchange-correlation functional was employed to fully each molecule. The double-numeric quality basis sets with polarization functions were used. The iterative tolerances for energy change, force, and displacements were 1×10^{-5} Ha, 0.002 Ha $Å^{-1,}$ and 0.005 Å, respectively. In the self-consistent field (SCF) procedure, 10^{-6} a.u. was used for the convergence standard electron density. After structure optimization, single-point energy calculation was executed. The HOMO, LUMO, and

ESP were outputted. The localized orbital locator (LOL) of the HATNQ molecule was calculated by VASP 6.3.0.

Energy storage mechanism calculation: DFT calculations were employed to calculate the Gibbs free energy (ΔG) of the reaction from pristine structure to structures 1, 2, 3, and 4. The generalized gradient approximation (GGA) with Perdew–Burke–Ernzerhof (PBE) exchange-correlation functional was employed to fully relax each structure. The double-numeric quality basis sets with polarization functions were used. The iterative tolerances for energy change, force, and displacements were 1×10^{-5} Ha, 0.002 Ha $Å^{-1,}$ and 0.005 Å, respectively. In the self-consistent field (SCF) procedure, 10^{-6} a.u. was used for the convergence standard electron density. The Gibbs free energy (ΔG) was calculated according to the following equation:

$$\Delta G = \Delta H - \Delta(T * S)$$

Here, ΔH is the enthalpy difference between the reactant and product, $\Delta(T*S)$ is entropy contribution energy. T is temperature (298.15 K), and S is entropy.

II. Supplementary Figures and Tables

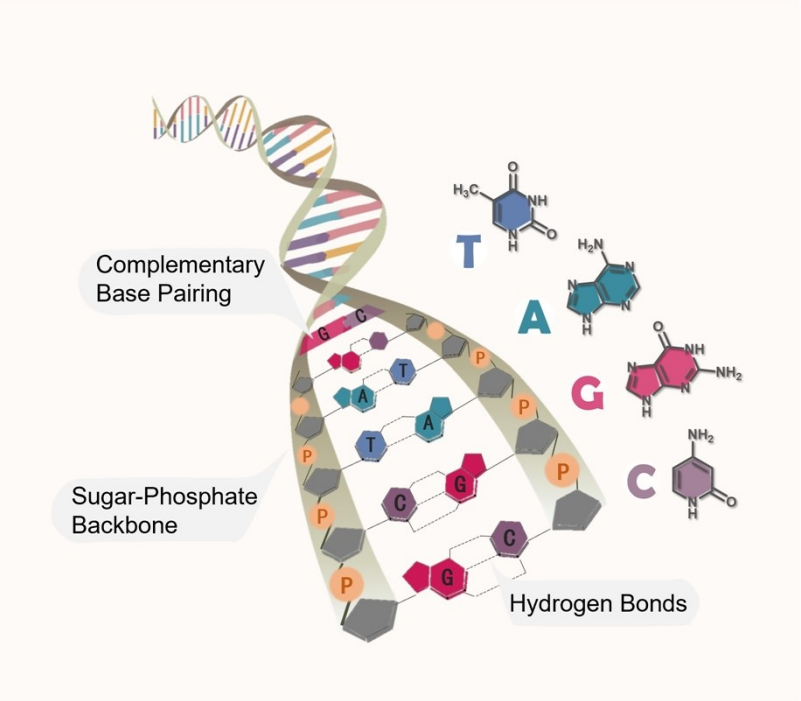

Figure S1. Chemical structures for the nucleobases in DNA.

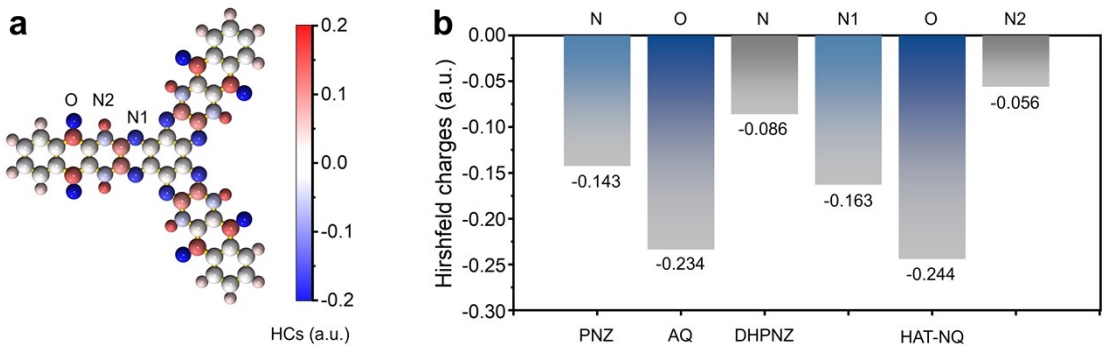

Figure S2. (a) Hirshfeld charges of HAT-NQ and (b) the corresponding charge distribution on O, N1, and N2 atoms.

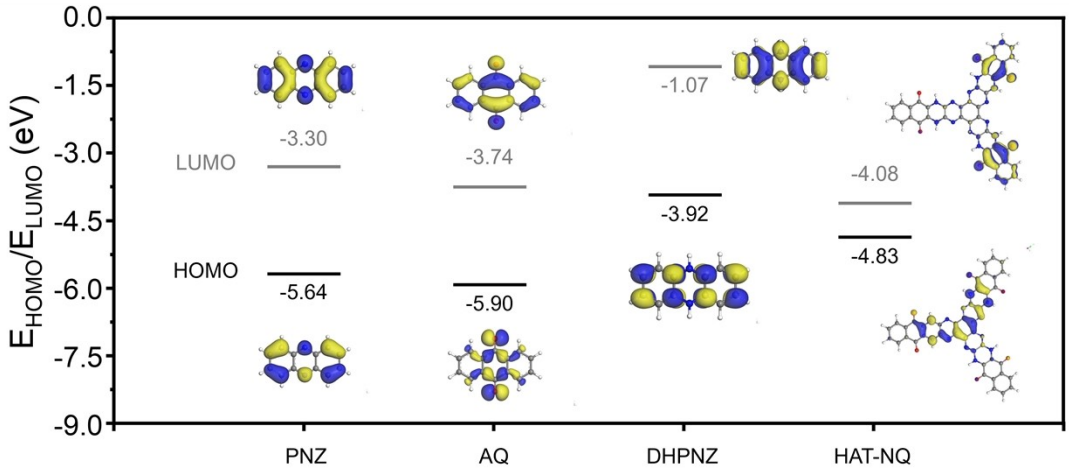

Figure S3. Calculated LUMO/HOMO energy levels of PNZ, AQ, DHPNZ and HAT-NQ.

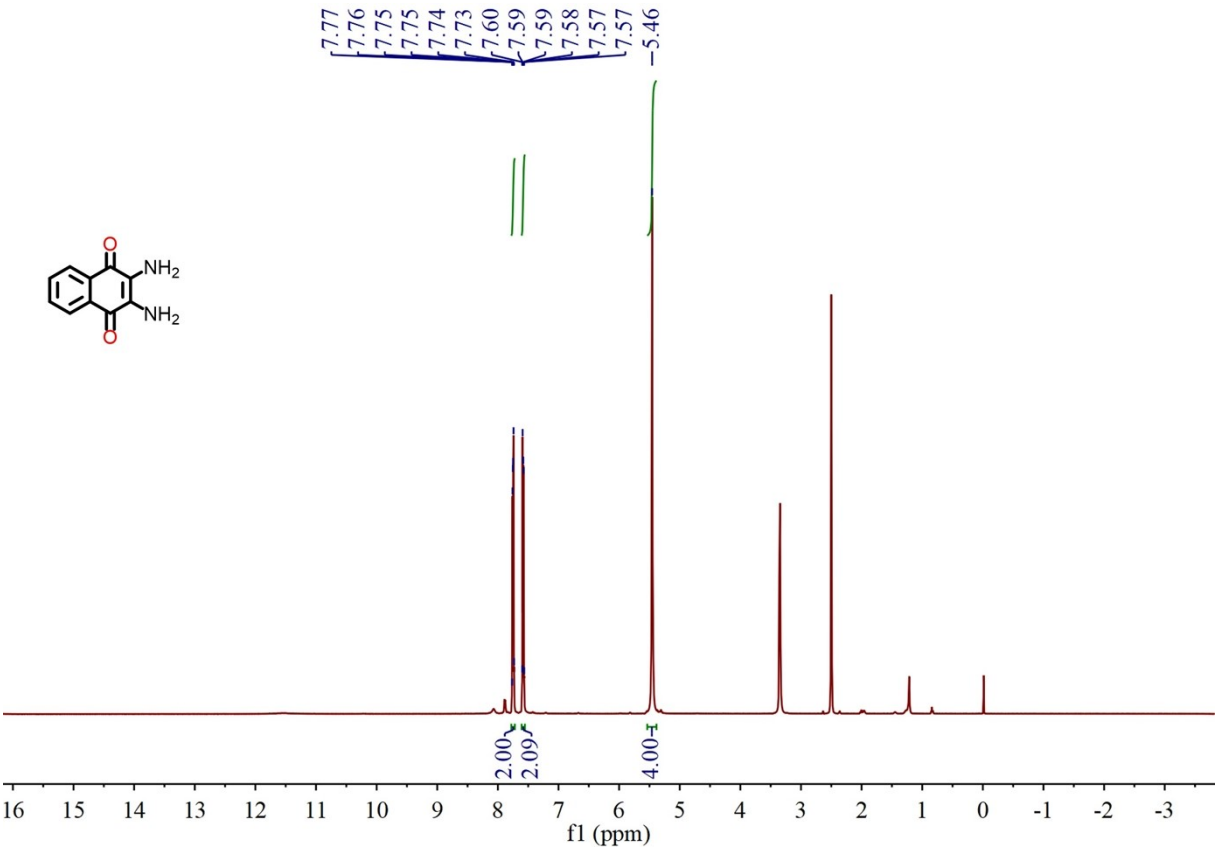

Figure S4. ^{1}H NMR (600 MHz, DMSO-d_6) spectrum of DANQ.

The ^{1}H NMR spectra of DANQ showed 3 distinct sorts of aromatic protons at 5.46 (s, 4H), 7.57-7.60 (m, 2H) and 7.73-7.77 (m, 2H) ppm, corresponging to the H atoms in -NH_2 and H atoms on the benzene, respectively. [1]

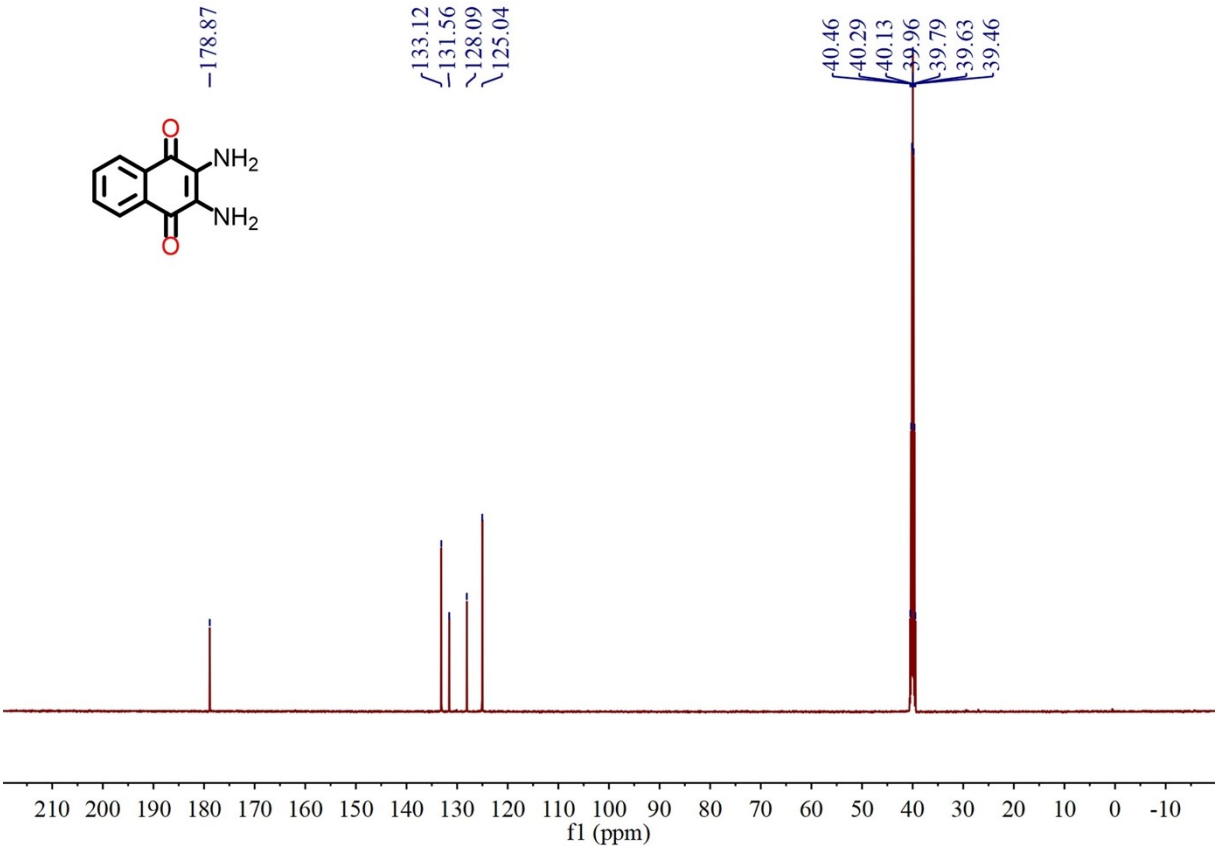

Figure S5. ^{13}C NMR (600 MHz, DMSO-d_6) spectrum of DANQ.

The ^{13}C NMR spectra of DANQ showed a signal at 178.87 ppm, corresponding to the C atoms in C=O groups. The peak at 133.12 ppm affirmed the existence of the -C-N bonds. The strong peaks at 131.56, 128.09 and 125.04 ppm were assigned to the C atoms on the benzene, respectively.

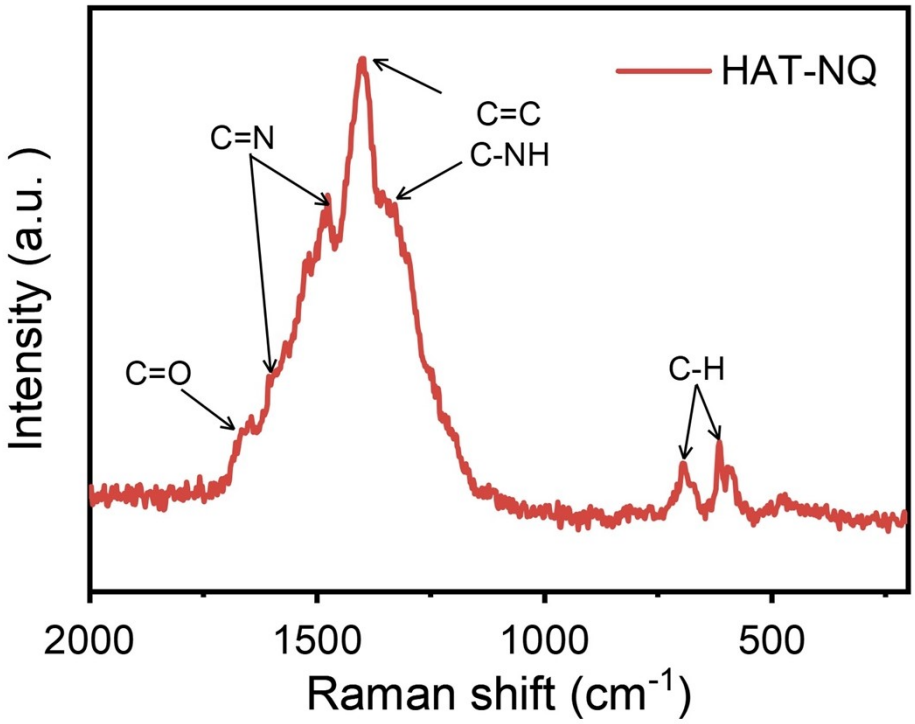

Figure S6. Raman spectrum of HAT-NQ.

The Raman spectrum demonstrates a series of characteristic peaks, which are designated to -C-H moieties on benzene ring (613, 690 cm^{-1}), -C-NH- (1352 cm^{-1}), -C=C- (1398 cm^{-1}), -C=N- (1473 and 1582 cm^{-1}) and -C=O-(1672 cm^{-1}). Meanwhile, the results agree with previous reports.[1-3]

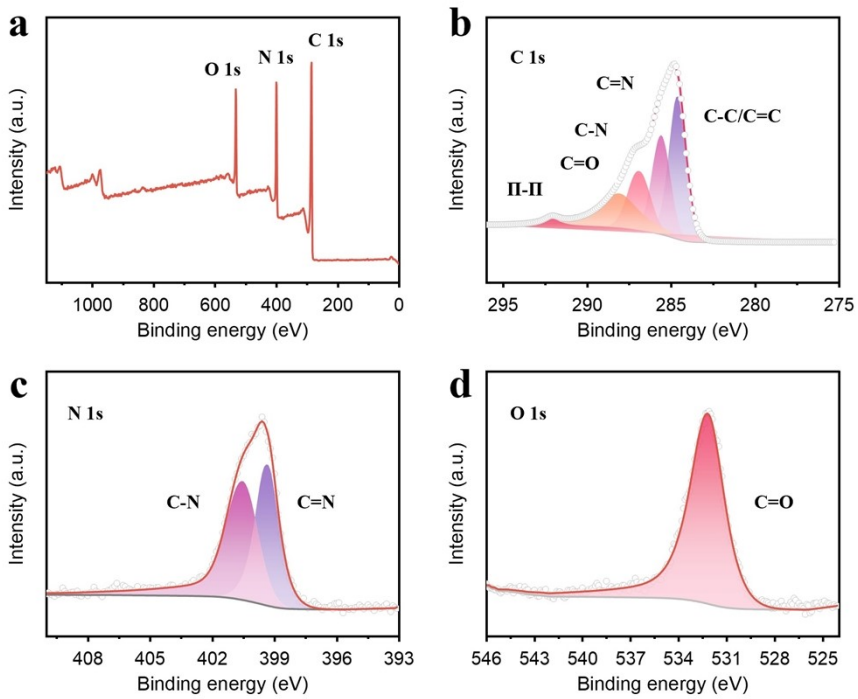

Figure S7. XPS spectra of HAT-NQ.

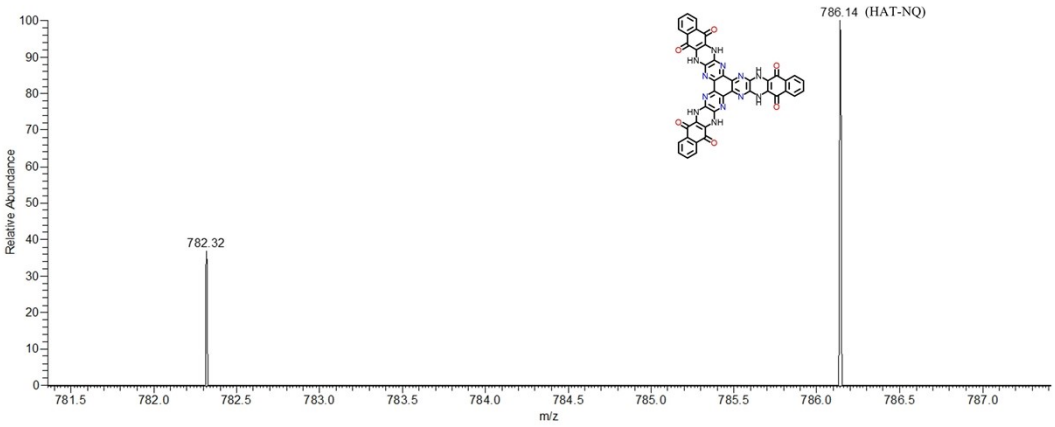

Figure S8. The high-resolution mass spectrometry of prepared HAT-NQ.

The m/z calculated for HAT-NQ of $C_{42}H_{18}N_{12}O_6$: 786.15; found: 786.14

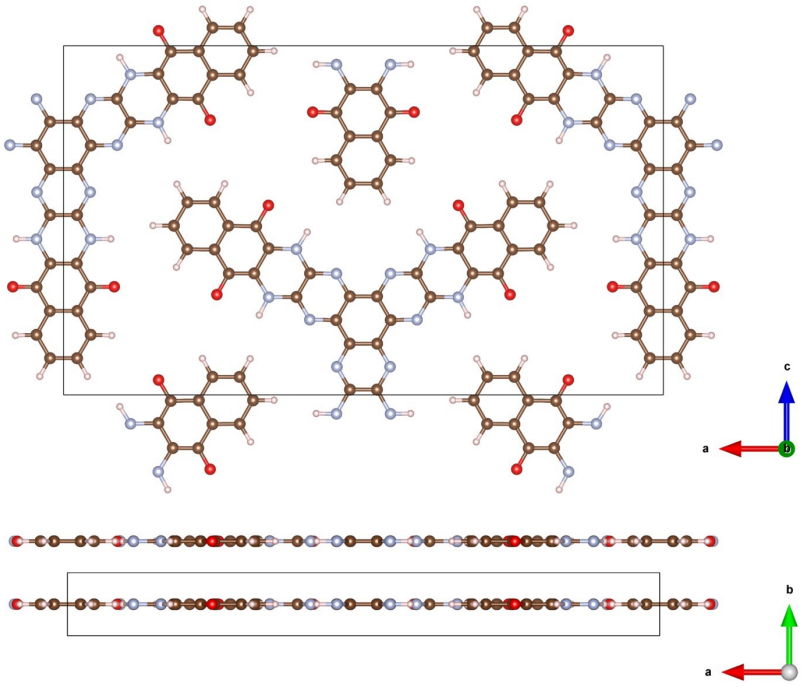

Figure S9. Pawley refinement crystal structure of HAT-NQ.

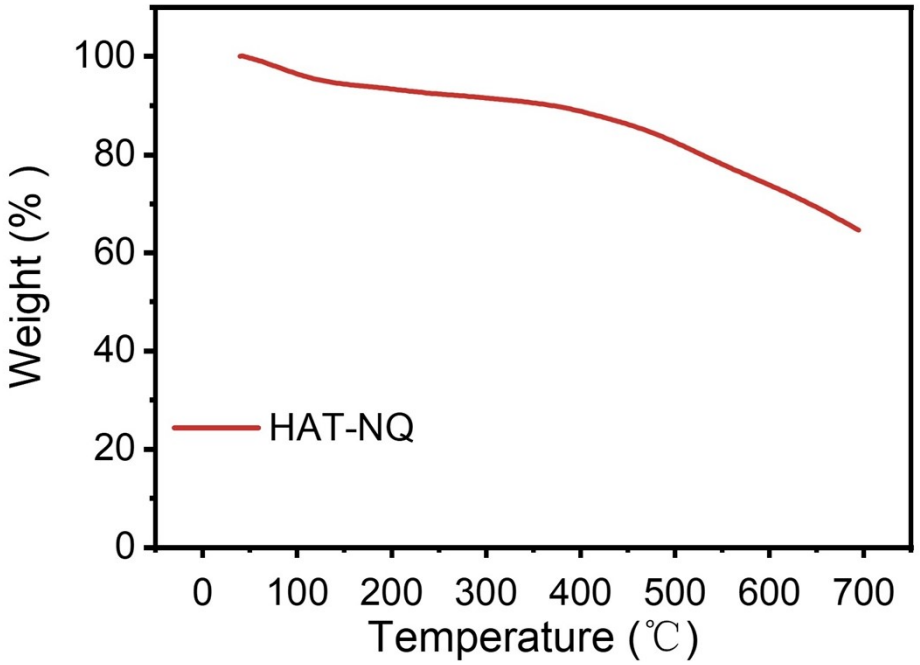

Figure S10. TGA curve of HAT-NQ.

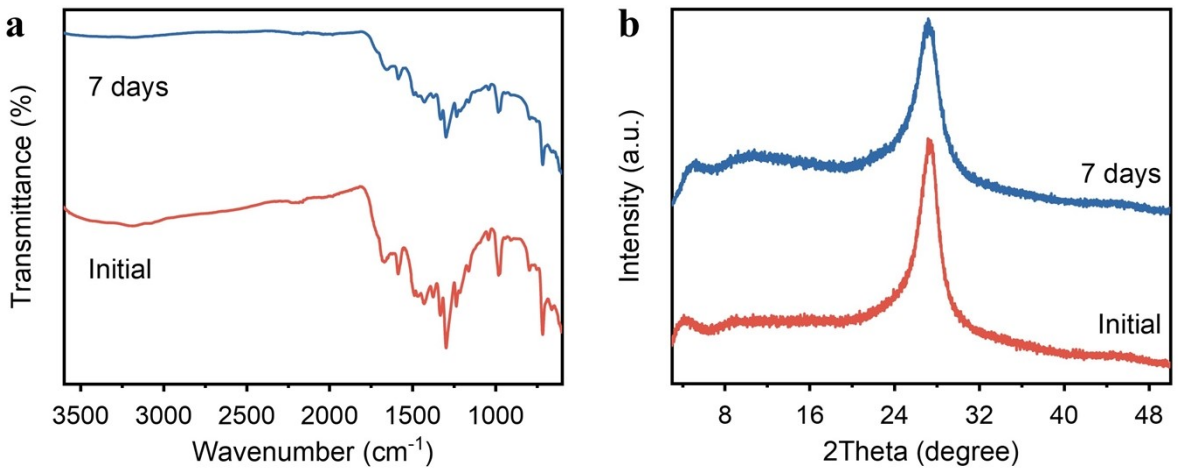

Figure S11. (a) FT-IR spectra and (b) XRD patterns of HAT-NQ after treatments under 2 M $ZnSO_4$ for 7 days.

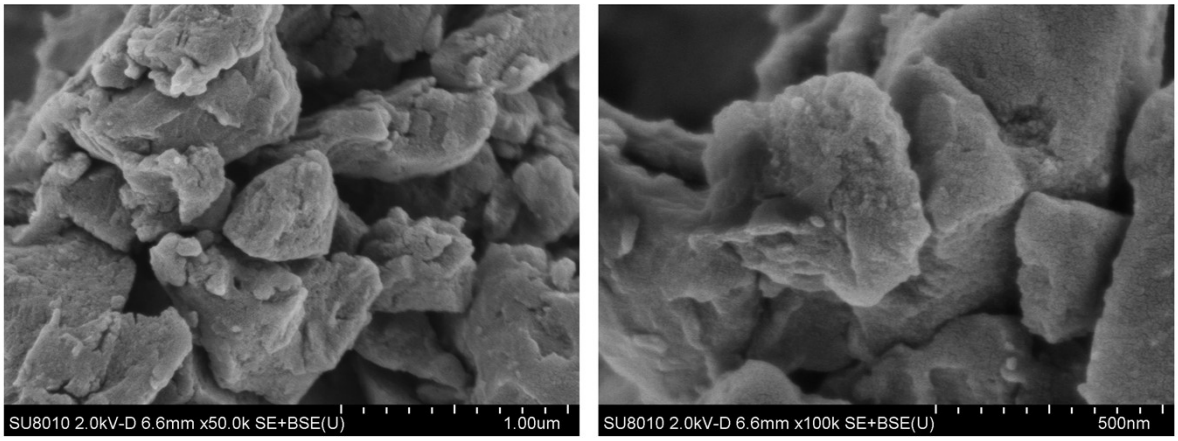

Figure S12. SEM images of HAT-NQ.

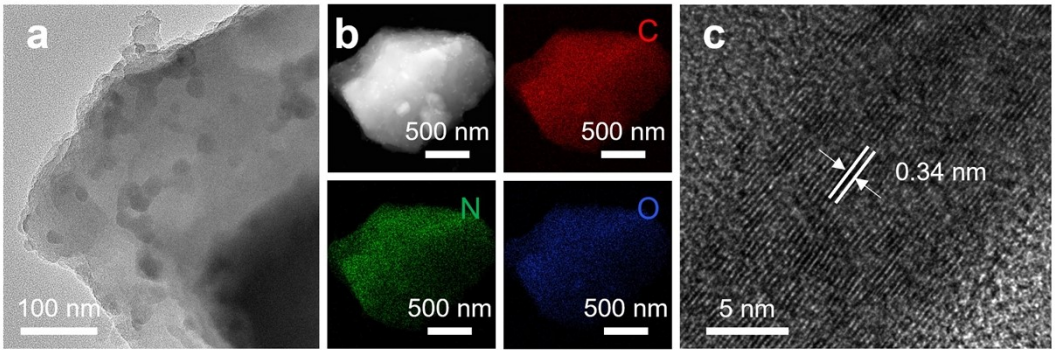

Figure S13. (a) TEM image, (b) HAADF-STEM and corresponding elemental mappings image, and (c) HRTEM image of HAT-NQ.

Morphological characterization reveals microstructured layer stacking (1-2 μm dimensions) with homogeneous C/N/O distribution. HRTEM directly confirms the 0.34 nm lattice spacing, aligning with XRD-derived crystallographic parameters.

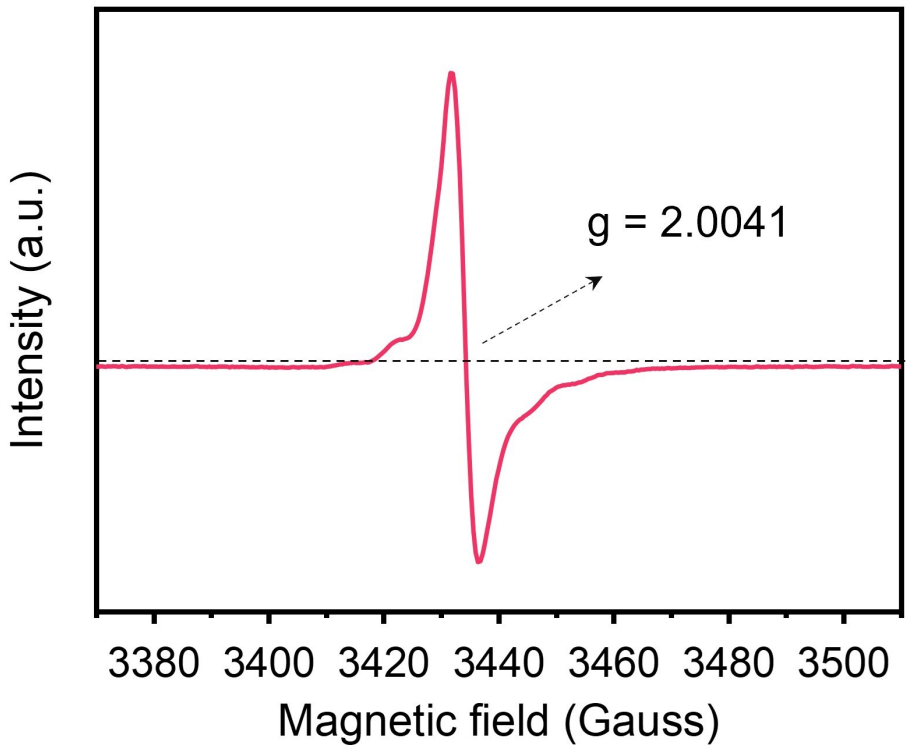

Figure S14. EPR spectrum of HAT-NQ.

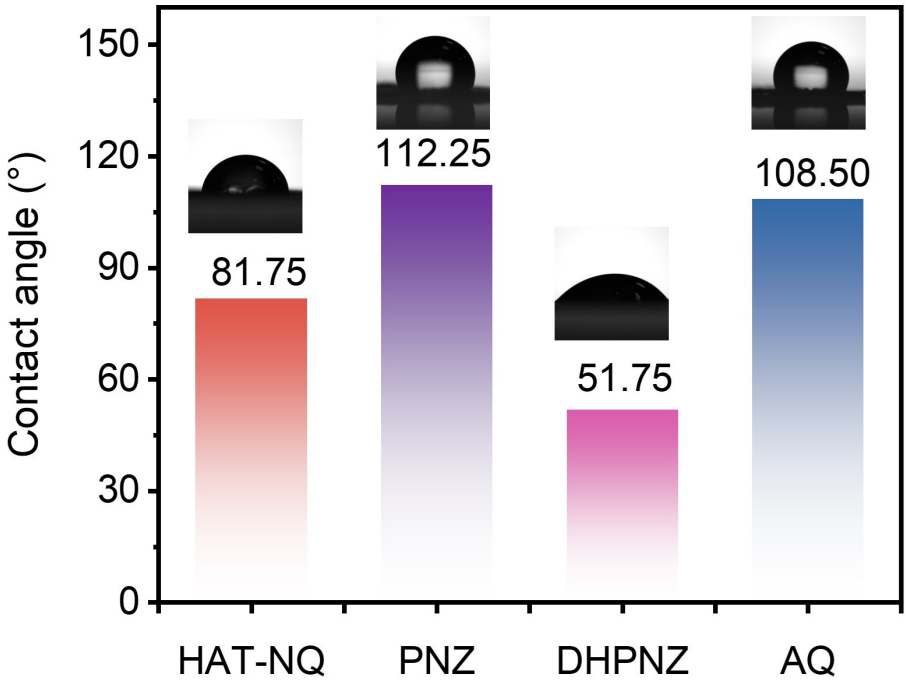

Figure S15. Contact angles of the electrolyte on different materials.

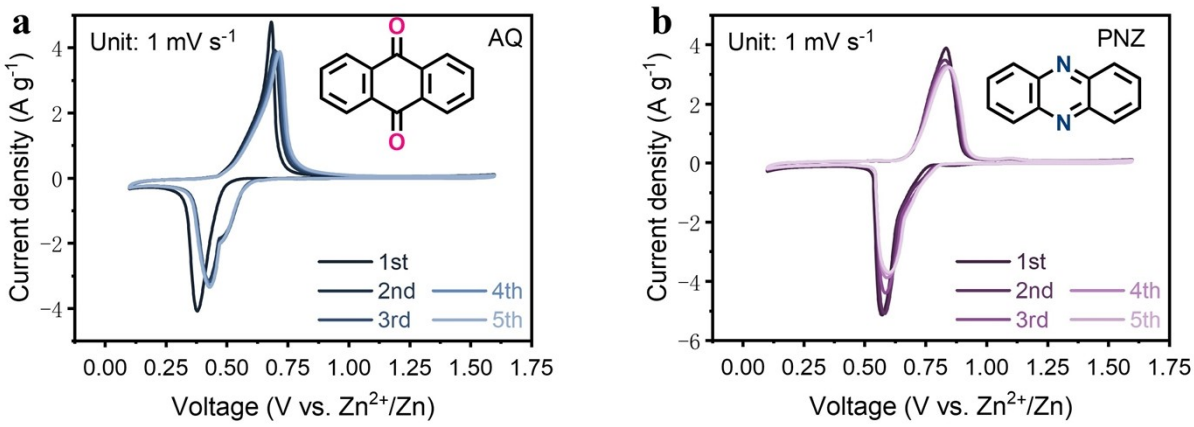

Figure S16. CV curves of (a) AQ and (b) PNZ.

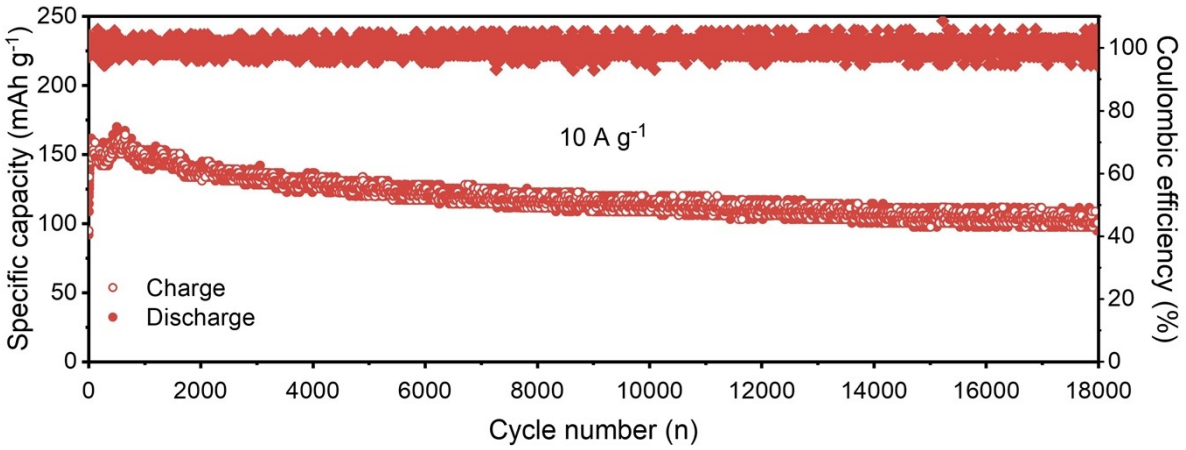

Figure S17. Long cycle performance of HAT-NQ at 10 A g^{-1}.

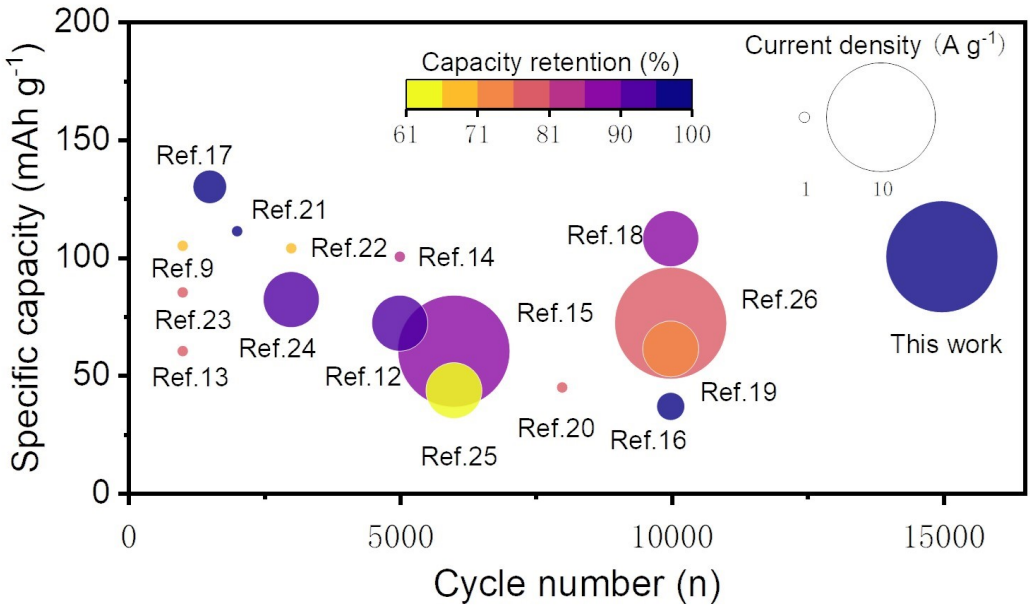

Figure S18. Comparative analysis of HAT-NQ with other aqueous Zn-organic batteries.

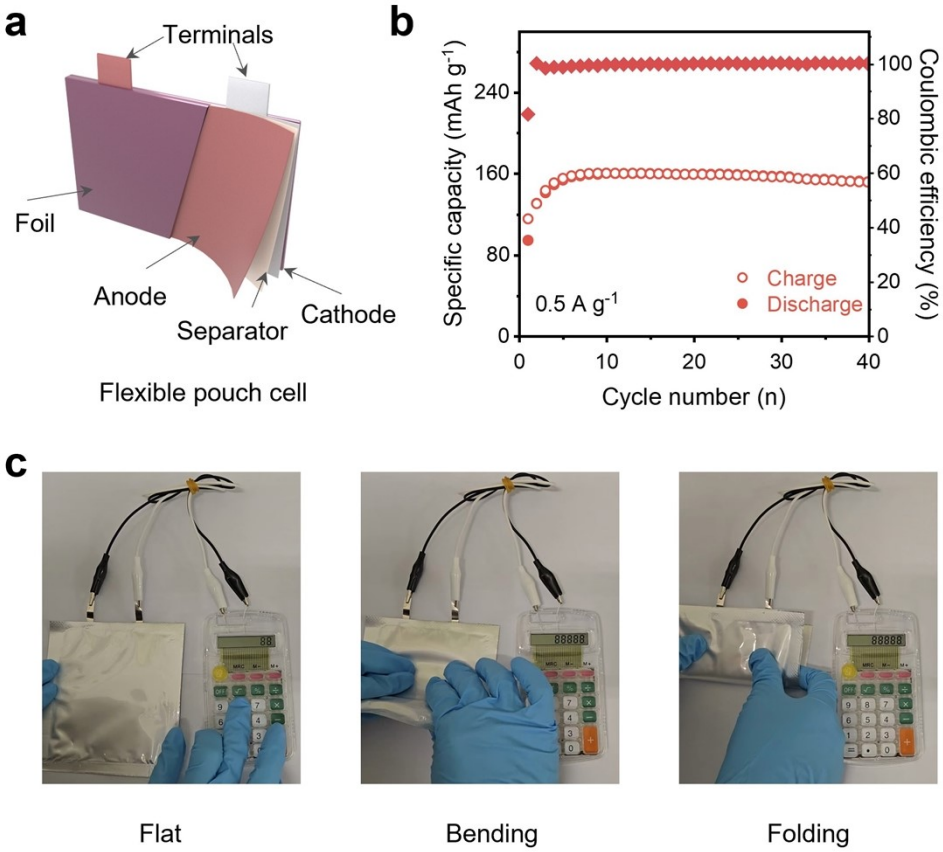

Figure S19. (a) The schematic of the assembled pouch cell. (b) The cycling performance of the pouch cell at 0.5 A g^{-1}. (c) The optical photograph of a calculator powered by a pouch cell.

To demonstrate its practical application, a pouch Zn//HAT-NQ cell was assembled, delivering an output capacity of approximately 160 mAh g^{-1} at 0.5 A g^{-1} and maintaining stable cycling for 40 cycles without significant attenuation. The pouch cells successfully powered a calculator and continued to function after various folding angles, highlighting their potential for use in electronic devices.

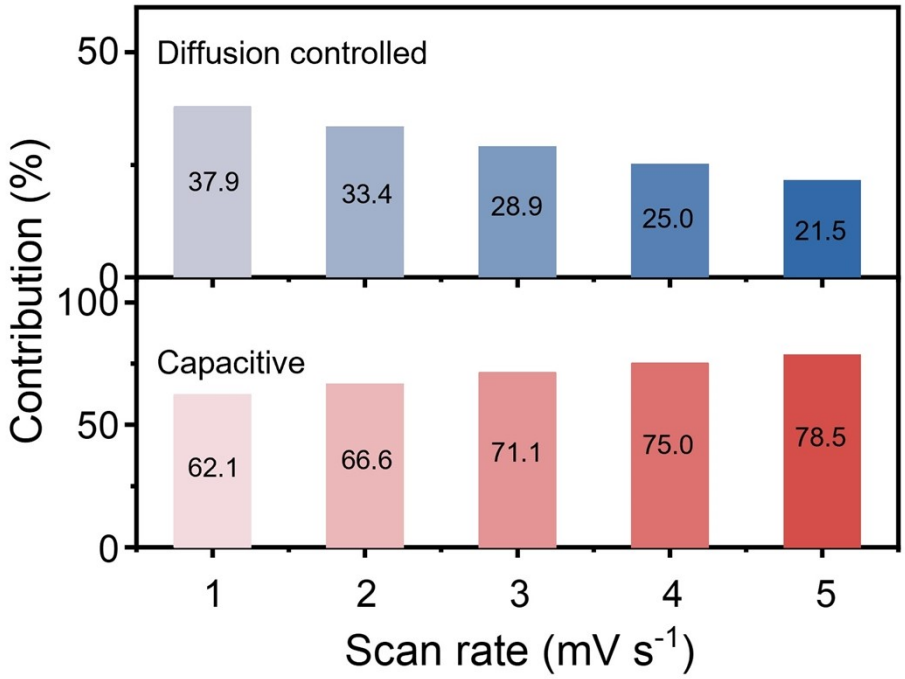

Figure S20. The capacitive contributions at various scan rates of HAT-NQ.

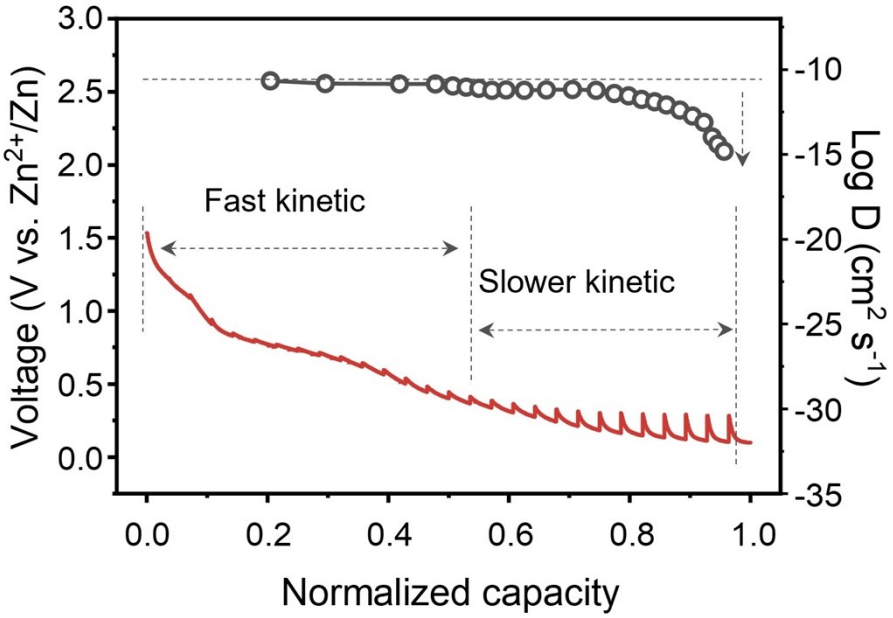

Figure S21. GITT curve and corresponding diffusion coefficient of HAT-NQ.

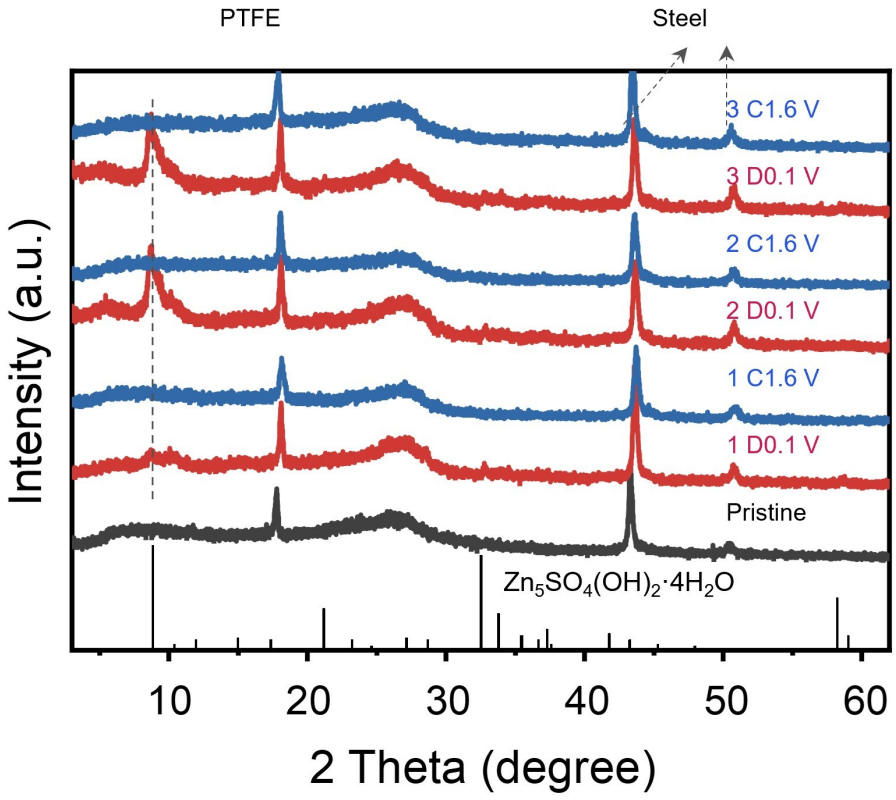

Figure S22. Ex-situ XRD patterns of HAT-NQ electrode at different states.

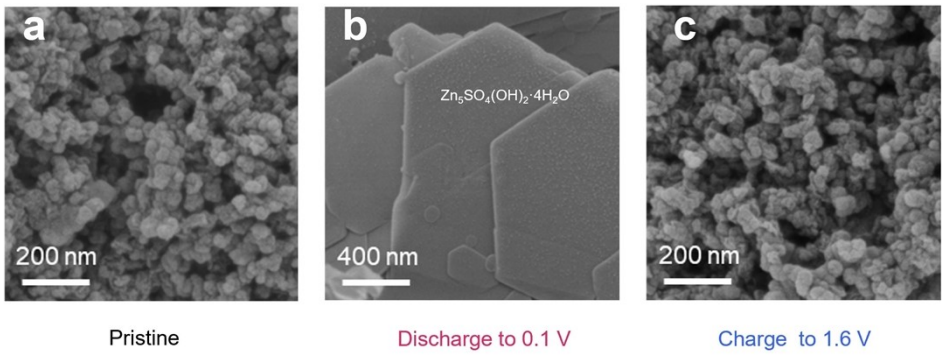

Figure S23. Ex-SEM images of HAT-NQ electrode at different states.

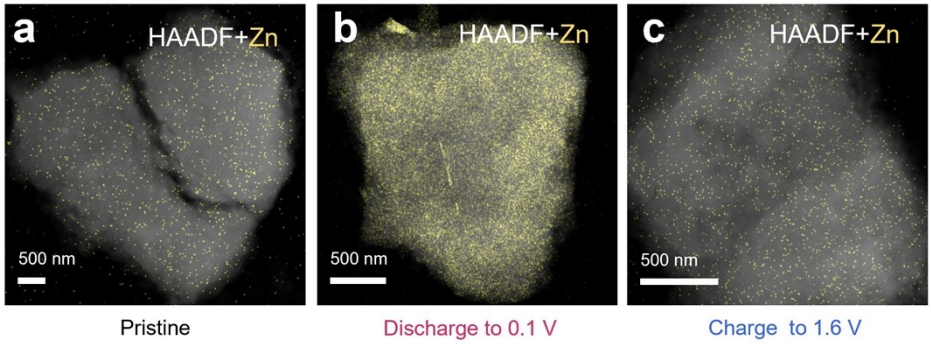

Figure S24. Ex-TEM images of HAT-NQ electrode at different states.

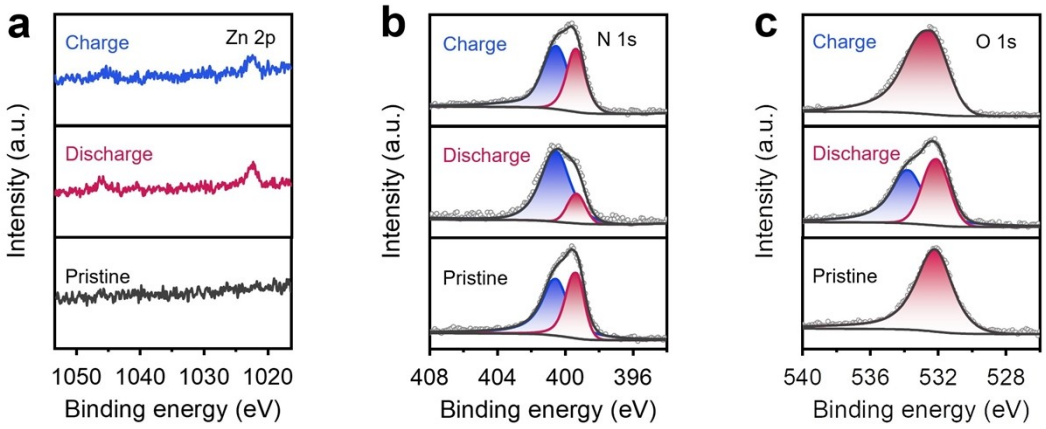

Figure S25. Ex-XPS analysis of (a) Zn2p, (b) N 1s, (c) O 1s of HAT-NQ electrode at different states.

Table 1. Zn elemental content of HAT-NQ electrode.

State	Element	Family	Atomic Fraction(%)	Atomic Error(%)	Mass Fraction(%)	Mass Error(%)	Fit error(%)
Pristine	C	K	91.18	2.68	88.92	1.66	0.64
	N	K	3.07	0.65	3.49	0.74	6.67
	O	K	5.71	1.16	7.42	1.50	1.68
	S	K	0.02	0.00	0.05	0.01	6.50
	Zn	K	**0.02**	0.00	0.11	0.02	5.29
Discharge to 0.1 V	C	K	78.13	4.41	64.39	2.28	0.64
	N	K	6.75	1.41	6.49	1.33	2.59
	O	K	10.98	2.29	12.06	2.46	1.79
	S	K	0.67	0.13	1.47	0.28	0.65
	Zn	K	**3.48**	0.50	15.60	2.15	0.27
Charge to 1.6 V	C	K	81.94	4.73	78.23	2.91	1.72
	N	K	10.23	2.13	11.39	2.32	1.92
	O	K	7.68	1.60	9.77	1.98	0.97
	S	K	0.05	0.01	0.12	0.02	1.82
	Zn	K	**0.10**	0.01	0.50	0.07	0.96
Wash with hydrochloric acid after discharge to 0.1 V	C	K	83.95	5.28	79.80	3.41	2.62
	N	K	8.05	1.68	8.92	1.82	2.22
	O	K	7.69	1.60	9.73	1.97	0.28
	S	K	0.04	0.01	0.11	0.02	2.13
	Zn	K	**0.28**	0.04	1.44	0.20	0.32

References

1. Z. Tie， Y. Zhang， J. Zhu， S. Bi and Z. Niu, *J. Am. Chem. Soc.,* 2022, **144**, 10301-10308.
2. Z. Tian， V. S. Kale， S. Thomas， S. Kandambeth， I. Nadinov， Y. Wang， W. Wahyudi， Y. Lei， A.-H. Emwas， M. Bonneau， O. Shekhah， O. M. Bakr， O. F. Mohammed， M. Eddaoudi and H. N. Alshareef, *Adv. Mater.,* 2024, **36**, 2409354.
3. L. Cheng， Q. Zhu， J. Liang， M. Tang， Y. Yang， S. Wang， P. Ji， G. Wang， W. Chen， X. Zhang and H. Wang, *ACS Appl. Mater. Interfaces,* 2021, **13**, 54096-54105.